A Benchmark of DC-DC Converters for DC Fast Charging Stations of Electric Vehicles

Honey Mol Mathew
Institute for Technical Physics (ITEP)
Karlsruhe Institute of Technology (KIT)
Karlsruhe, Germany
honeymol.mathew@kit.edu

Gabriele Arena
Institute for Technical Physics (ITEP)
Karlsruhe Institute of Technology (KIT)
Karlsruhe, Germany
gabriele.arena@kit.edu

Andrii Chub
Power Electronics Research Group
Tallinn Institute of Technology (TalTech)
Tallinn, Estonia
andrii.chub@taltech.ee

Giovanni De Carne
Institute for Technical Physics (ITEP)
Karlsruhe Institute of Technology (KIT)
Karlsruhe, Germany
giovanni.carne@kit.edu

Dmitri Vinnikov
Power Electronics Research Group
Tallinn Institute of Technology (TalTech)
Tallinn, Estonia
dmitri.vinnikov@taltech.ee

Mykola Lukianov
Faculty of Electrical Engineering
Gdańsk University of Technology
Gdańsk, Poland
mykola.lukianov@pg.edu.pl

***Abstract*—The introduction of 800 V electric vehicles on the market creates the need for universal chargers that can interface electric vehicles with different battery voltages. In particular, this paper focuses on DC-DC converters for DC fast charging stations with a wide output voltage range to match the requirements of both 400 V and 800 V electric vehicles. A comparative analysis of two emerging topologies and a traditional dual active bridge has been conducted to evaluate the efficiency of these converters over an output voltage range of 200-1000 V. This study includes an assessment based on two different charging profiles for electric vehicles, specifically targeting 400 V and 800 V battery systems.**

I. Introduction

The transition to sustainable energy sources is being accelerated by the growing adoption of electric vehicles (EVs), which increases demand for clean energy and reduces dependence on fossil fuels. However, the spread of electric vehicles has always been limited by the so-called "range anxiety" issue. In fact, EVs do not provide the same distance range as internal combustion engine vehicles (ICEVs). Moreover, EV charging stations are less common than gas stations, and EV charging requires a longer time than the one required to refuel traditional ICEVs. One way to tackle this problem could be achieved by a huge breakthrough in battery technologies. The other way is to create a wide network of DC fast charging stations all over the countries, which this research work targets [1].

Electric vehicles with 800 V powertrains are now available, offering higher charging rate. By increasing the internal voltage, these EVs limit the charging current while still allowing high charging speeds. This results in shorter charging times and better efficiency [2], [3]. However, 800 V EVs are not compatible with DC fast chargers that were originally designed for 400 V EVs, which makes them require an additional 1:2 DC-DC converter [4]. Moreover, traditional DC-DC converters adopted in DC fast charging stations, like dual active bridge (DAB) converters, are unsuitable for interfacing both 400 V and 800 V EVs. Hence, introducing 800 V EVs on the market creates the need for universal chargers equipped with emerging DC-DC converters capable of interfacing both traditional 400 V and new 800 V EVs. This paper aims to create a benchmark of emerging DAB-based DC-DC converter topologies that can provide a wide output voltage range.

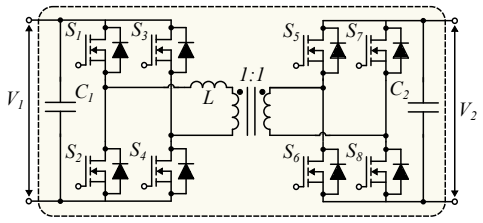

Fig. 1: Dual active bridge.

II. DAB based - Converter Topologies

DAB is well known for its high efficiency and high power density, and it is one of the most adopted topologies in DC microgrids, aerospace, and EV charging [5]–[7]. DAB is made by two full bridges galvanically isolated by a high- or medium-frequency transformer which can be shown in Fig 1. Using the most typical single phase shift (SPS) modulation, the duty ratio of each leg of the two full bridges is 50 %. The power delivered by the DAB is determined by the phase shift between the two full bridges, as stated by the following equation:

$$P = \frac{nV_1V_2\varphi(\pi - \varphi)}{2\pi^2 f_s L}, \tag{1}$$

where n is the turn ratio of the transformer, V_1 and V_2 are the first and second DC voltage of the converter, respectively, φ is the phase shift between the two full bridges of the DAB, f_s is the switching frequency, and L is the inductor in series with the transformer winding.

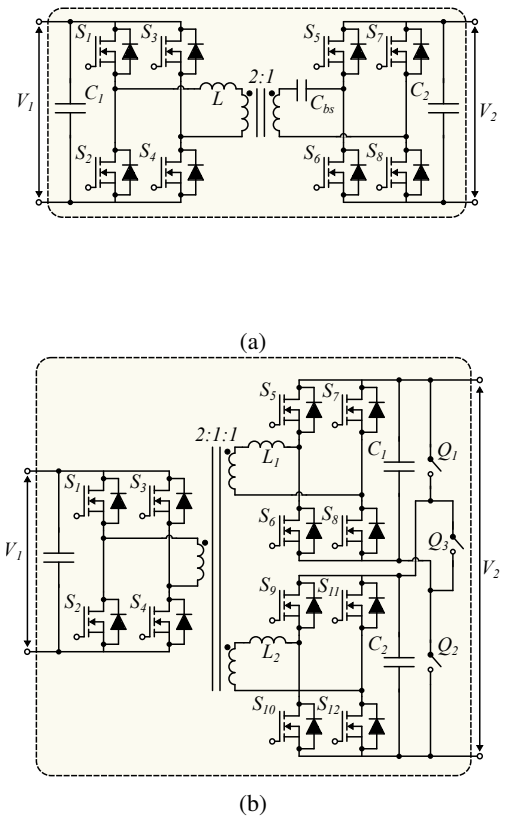

Fig. 2: Emerging topologies analyzed in this research work. (a) DAB-based topology with secondary DC blocking capacitor enabling the quasi-SPS modulation (S_7=OFF, S_8=ON, (reconfigurable converter 1)). (b) DAB-based converter with two outputs that can be connected in parallel or in series (reconfigurable converter 2).

The DAB-based topology proposed in [8] is a DAB converter with a so-called quasi-SPS modulation. In particular, the right leg of the second full bridge has a different modulation. Its upper switch is continuously off, whereas its lower switch is continuously on. The quasi-SPS modulation technique extends the ZVS range of the DAB by a factor of 2. However, it requires a DC-blocking capacitor C_{bs} to avoid the saturation of the transformer, as shown in Fig. 2a. The power of a DAB using the quasi-SPS modulation is half of the power transferred during the SPS modulation:

$$P = \frac{nV_1V_2\varphi(\pi-\varphi)}{4\pi^2 f_s L},\ V_{cb} = \frac{V_2}{2}, \tag{2}$$

where V_{cb} is the voltage of the blocking capacitor on the secondary side of the transformer.

The DAB-based converter proposed in [9] comprises two full bridges on the secondary side, which can be connected in parallel or series to interface 400 V and 800 V EVs, as shown in Fig. 2b. Moreover, a three-winding transformer is used to connect the three full bridges. The output current of the converter is the sum of the output currents of the two output bridges when working in parallel mode (P-mode), whereas it is the same of the two output bridges when working in series mode (S-mode). However, the output voltage is the same of the two output bridges in P-mode and it is the sum of the voltage of the two output bridges in S-mode. This structure allows to keep high efficiency without using two DAB converters connected in parallel/series configuration.

TABLE I: Variables for the thermal calculation of the SiC-MOSFET

Parameters	**Variables**	**Minimum**	**Maximum**
Device voltage	v	0	800 V
Device current	i	0	50 A
Junction temparature	T	0	175
Gate(on)Resistance	$R_{g\ on}$	2	120
Gate(off)Resistance	$R_{g\ off}$	2	120

III. Loss Anaylsis of the DC-DC Converter Topologies

In the DAB configuration, the primary components include semiconductor switches, inductors, and high-frequency transformers, where most of the losses originate.

A. Thermal analysis of MOSFET

In power converters, most of the power losses come from switching devices, resulting from a combination of conduction and switching losses [10]. The switching losses can be defined as:

$$P_s = \frac{1}{2}V_{DS}I_D(t_r + t_f)f_s, \tag{3}$$

where V_{DS} represents the drain-source voltage, I_D denotes the drain current, t_r and t_f are the rise and fall time of the switching devices, respectively. On the other hand, the conduction losses are defined as:

$$P_{cond,\,on} = R_{on}I_D^2, \tag{4}$$

where R_{on} is the on-resistance of the switching devices.

The analysis of the DAB-based converters employed the Infineon IMBG120R030M1H MOSFET, which has a rated voltage of 1200 V and a current capacity of 56 A. The SiC-MOSFET operates at a switching frequency of 100 kHz, and the evaluations were conducted using PLECS software. SiC's higher critical field strength and thermal conductivity allow for efficient high-voltage operation with low conduction losses. At 100 kHz, passive components like inductors and capacitors are smaller, reducing the converter size and increasing power density [11]. The main variables that are used for the thermal loss calculations of MOSFET are given in TABLE I. Fig. 3a demonstrates that the conduction losses of a single IMBG120R030M1H MOSFET are more sensitive to

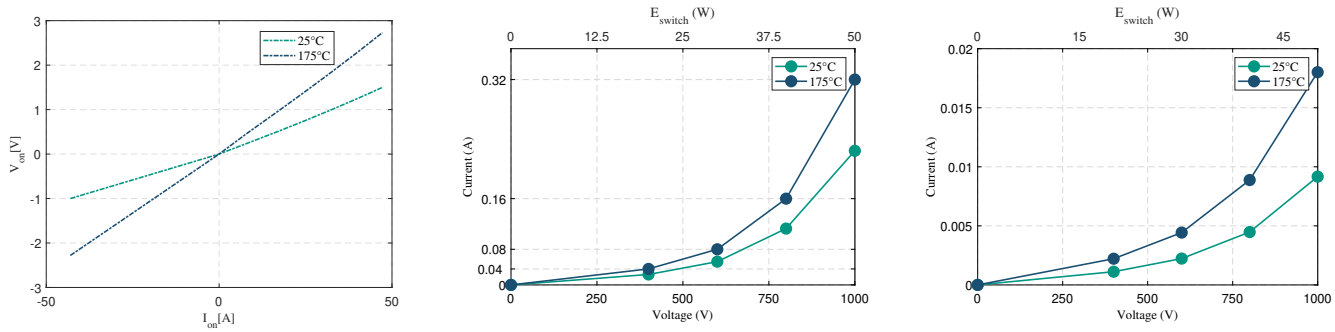

(a) (b) (c)

Fig. 3: Semiconductor losses of the three converters. (a) Conduction losses. (b) Turn-on losses. (c) Turn-off losses.

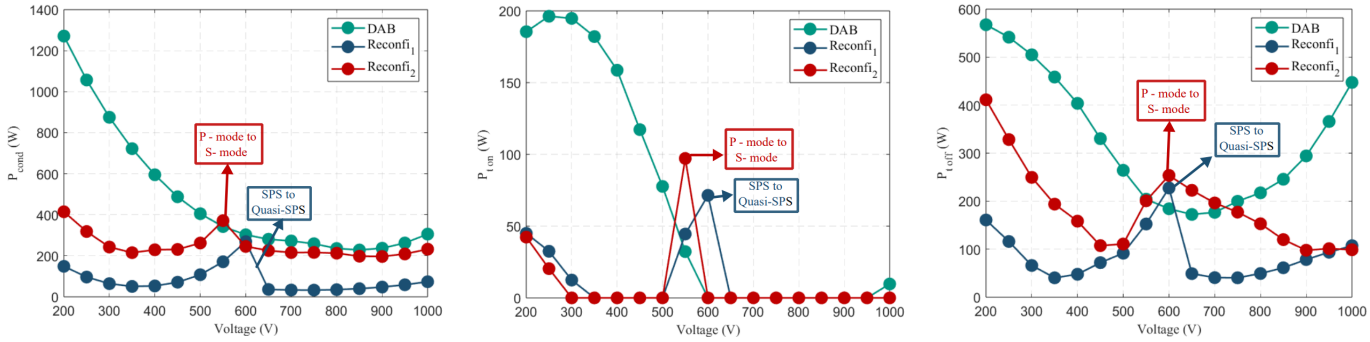

(a) (b) (c)

Fig. 4: Semiconductor losses of the three converters. (a) Conduction losses. (b) Turn-on losses. (c) Turn-off losses.

temperature fluctuations than switching losses. As the temperature rises, conduction losses increase significantly, reaching approximately 1 V at 50 A when the temperature is 175°C.

In a MOSFET, switching loss includes both turn-on and turn-off losses. During the turn-on phase, the channel current (i) is crucial; as the temperature (T) increases, the elevated channel current results in a higher di/dt, leading to increased drain current and higher switching losses, as shown in Fig. 3b Conversely, during the turn-off phase, the displacement current through the drain-source and source capacitances exceeds the channel current. This causes parasitic capacitance to dominate the turn-off characteristics, while the junction temperature (T_j) has minimal impact, resulting in only a slow increase in power losses during the turn-off transient, as illustrated in Fig. 3c [12].

In numerous instances, power dissipation can be calculated by finding the average power dissipation of individual semiconductors. The process for calculating average losses for a component involves summing the losses experienced throughout a switching cycle and then generating an average power pulse for the following switching cycle. This analysis compares the thermal losses of two reconfigurable DAB-based converters with those of a conventional DAB, designed for DC fast charging of 400 V and 800 V EVs using 100 kHz SiC MOSFETs. The key parameters for the thermal analysis of the DAB-based converters are presented in TABLE I and TABLE II. Different leakage inductances are chosen to improve converter efficiency by helping with soft-switching, reducing current ripple, and ensuring ZVS, based on the voltage level of the charging application. Reconfigurable converter 1 operates at 30 kW up to 550 V and then shifts to quasi-single phase shift modulation beyond that and cutting the power into half, which is 15 kW. Reconfigurable converter 2 acts like a standard DAB up to 550 V, but beyond that, it switches to series mode. In the case of reconfigurable converter 2, in series mode, the turns ratio becomes 2:1, involving an additional bridge and increasing the switch count to 12. Fig. 4a illustrates the comparison of conduction losses among the converters. The conventional DAB shows higher losses compared to both

TABLE II: Converter specifications

Specifications	DAB	Converter 1	Converter 2
Power	30 kW	30 kW	30 kW
Input voltage	800 V	800 V	800 V
Frequency	100 kHz	100 kHz	100 kHz
Turns ratio	1:1	2:1	2:1
L_1	11.60 μH	25.51 μH	57.99 μH
L_2	N.A.	N.A.	57.99 μH
C_{bs}	N.A.	22 μF	N.A.
Number of switches	8	8	12
Switch	SiC-MOSFET	SiC-MOSFET	SiC-MOSFET

reconfigurable converters. Notably, reconfigurable converter 1 demonstrates better efficiency. The conventional DAB experiences elevated conduction losses at lower voltages due to SiC MOSFETs, peaking at around 1200 W and decreasing to approximately 200 W at 600 V. In contrast, reconfigurable converter 1 starts with around 100 W of losses, significantly lower than the conventional DAB, especially during single-phase shift modulation at 30 kW. The transition to quasi-single phase shift modulation beyond 550 V results in a minor spike in losses, followed by a declining trend. Reconfigurable converter 2 exhibits lower losses than the conventional DAB but slightly higher losses than reconfigurable converter 1, with a minor increase in losses observed during the transition from parallel to series mode between 550 V and 600 V. Fig. 4b and 4c depicts the turn-on and turn-off losses of the three converters. The turn-on losses are smaller than the turn-off losses for all converters. The conventional DAB has the highest turn-on and turn-off losses, while reconfigurable converter 1 has the lowest. Generally, the DAB-based converters operate near zero voltage conditions for turn-on losses, except during lower voltage ranges and transitions to quasi-SPS modulation in reconfigurable converter 1 and from parallel to series mode in reconfigurable converter 2.

B. Trasformer Loss calculation

TABLE III: Core parameters to calculate the number of turns

Parameters	**Variables**	**Values**
Maximum magnetic flux density	B_{max}	0.1 T
The effective cross-section area of one core	A_e	448 mm^2
Effective permeability of the core	μ_e	2578
Inductance factor for one core	A_L	4100
Core Volume	V_e	159 cm^3
Number of cores 'UU'	N	4
Power loss density	P_d	71.08 mW/cm^3

The transformer core losses have also been taken into account in this work. In particular, the time-average core losses per unit volume of the core with non-sinusoidal flux waveforms are estimated using the improved generalized Steinmetz equation (iGSE) [13]:

$$\overline{P_v} = \frac{k_i(\Delta B)^{(\beta-\alpha)}}{T} \sum_j \left(\left| \frac{V_j}{nA_c} \right| \right)^{\alpha} (\Delta t_j), \tag{5}$$

where α and β are the Steinmetz coefficients, k_i is another value depending on the Steinmetz coefficients, ΔB is the peak-to-peak flux density, T is the total period of the periodic waveform, V_j represents the j^{th} winding voltage, A_c is the cross-sectional core area, and Δt_j is the j^{th} time length where the winding voltages are constant. The material of high-frequency transformer used in DAB is N95 which is a Ferrite MnZn magnetic material. The core used for the transformer for the loss calculation is a 'UU' core. Then by combining 'UU' cores, 'EE' cores are made. UU cores are favored for their simplicity, high window utilization, and ease of cooling. Their straightforward design aids manufacturing, while efficient heat dissipation and optimal winding space usage make them advantageous for enhancing transformer reliability, performance, and power density. [14]. The main parameters used to find the number of turns can be seen in Table III. Moreover, by using the switching frequency, the primary voltage v_p, and secondary voltage v_s, the number of turns on the transformer can be calculated.

The next step in the transformer losses calculation is to estimate the winding area for the primary and the secondary winding. The area of the primary side winding can be calculated by using equation 6 where I_1 represents the current through the primary side and N_1 is the number of turns of the primary side. From practical experience, it is considered that the current density is 3 mm^2 and a fill factor of 0.4.

$$A_{winding1} = \frac{I_1\ N_1}{I_d\ f_f} = \frac{75\ \text{A} \cdot 12}{3\ \text{A/cm}^2 \cdot 0.4} = 750\ \text{mm}^2, \tag{6}$$

where I_d is the current density and f_f is the fill factor.

The area of the secondary side winding can be calculated by using equation 7 where I_2 represents the current through the secondary side and N_2 refers the number of turns of the secondary side.

$$A_{winding2} = \frac{I_2\ N_2}{I_d\ f_f} = \frac{150\ \text{A}\ 6}{3\ \text{A/cm}^2 * 0.3} = 750\ \text{mm}^2 \tag{7}$$

Then, by using the variables in TABLE III and calculating the power loss density from a Ferroxcube excel sheet that uses the iGSE, the magnetic core losses can be calculated as follows:

$$P_{losses\ core} = V_e\ N\ P_d \tag{8}$$

where V_e is the core volume and P_d is the power loss density.

The core losses of the high-frequency transformer used in DAB with 100 kHz frequency is calculated as 40 W.

The copper losses of the transformer have been found by considering the windings' DC resistance:

$$R = \rho \frac{l}{A} \tag{9}$$

where ρ is the electrical resistivity of the copper, l is the length of the turns, and A is their cross-sectional area.

DC fast charging stations are typically equipped with 20 kW, 30 kW, or 50 kW modules. So, 30 kW modules have been designed in this paper to compare the three converters. Their parameters are listed in TABLE II.

IV. Efficiency Analysis Under Different Charging Profiles

Analyzing the charging profile is crucial for understanding how power is transferred from the charger to the battery and the amount of energy delivered during the process, which ultimately impacts the efficiency of the DAB-based converters.

The Fig. 5a illustrates the charging profile of Tesla's 250 kW charger alongside a DAB-based converter with a 30 kW capacity. The SoC not only dictates the amount of energy needed to be transferred to the battery but also

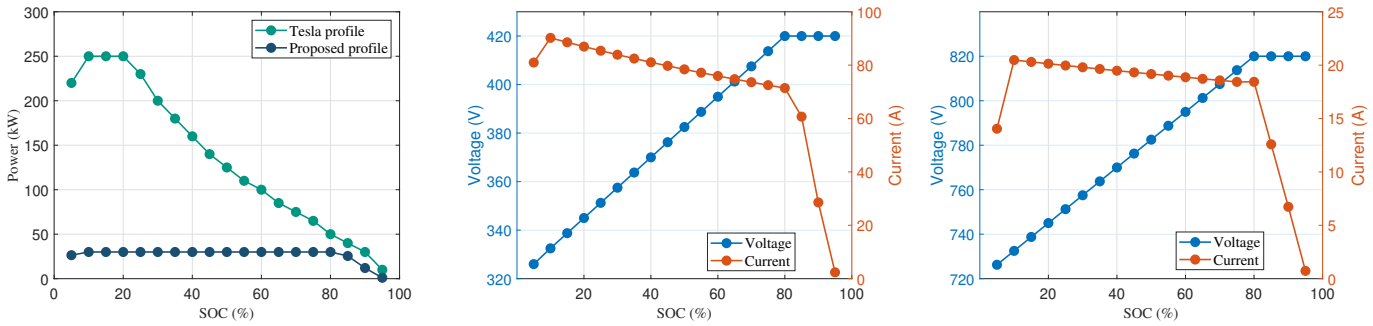

(a) (b) (c)

Fig. 5: Battery charging profile. (a) Power vs SOC. (b) Voltage and current vs SOC forr 400 V battery (c) Voltage and current vs SOC for 800 V battery.

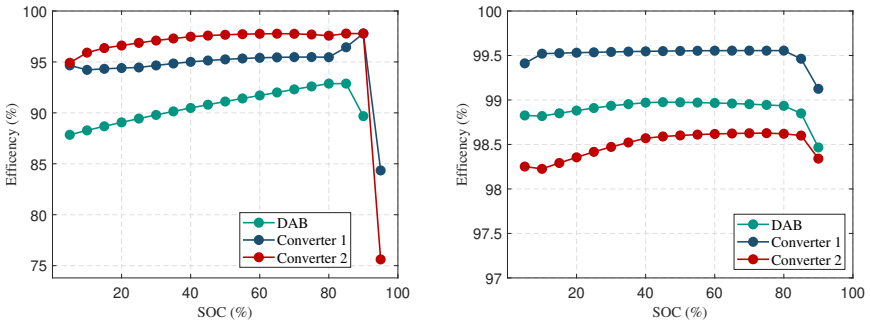

(a) (b)

Fig. 6: Efficency analysis of DAB-based converters(a) Efficency of DAB based converters for 400 V charging profile (b) Efficency of DAB based converters for 800 V charging profile

influences the power transfer capability of a converter [15]. The Tesla charger employs the CC-CV (Constant Current-Constant Voltage) charging method for Li-ion batteries. The charging process begins in CC mode when the SoC reaches around 5%, with the power transfer gradually increasing from 220 kW to 250 kW as the SoC reaches 10%. Beyond this point, up to 30% SoC, the power transfer capability remains constant at around 250 kW. However, once the SoC surpasses 30%, the charger transitions to CV mode, resulting in a gradual decrease in current and a corresponding reduction in power transfer to prevent overcharging. In contrast, DAB-based converters follow a similar CC-CV charging strategy but exhibit differences in their charging profiles. In particular, their charging behavior is constant-power based like on-board chargers due to their lower power rate. At 10% SoC, these converters enter the CC mode, delivering a constant power transfer of 30 kW up to 80% SoC. During this phase, the power transfer remains steady to ensure efficient charging. Upon reaching 80% SoC, the converter switches to CV mode, resulting in a gradual reduction in current and a corresponding decrease in power transfer to avoid overcharging the battery. The higher the power and the current, the lower the SoC level in which the CV mode is reached.

In electric vehicles, lithium-ion batteries are charged using the CC-CV method. The nominal voltage of these batteries typically stands at 4.3 V. At 10% SoC, the voltage is approximately 3.2 V, while at 80% SoC, it reaches the maximum voltage of 4.3 V. By combining these lithium-ion cells in series and parallel configurations, the battery voltage can be adjusted to either 400 V or 800 V. Using the proportionate method, the corresponding voltage for each SoC level can be determined when the battery voltage is increased. DAB-based converters operate at around 30 kW and its variation concerning SoC of the battery is shown in Fig. 5b. The current can be calculated by dividing the power by the voltage corresponding to the SoC level which is depicted in Fig. 5b. In the case of a 420 V battery profile in Fig. 5b, the battery voltage increases linearly from 320 volts at 5% SoC to a maximum of 420 volts at 80% SoC. On the other hand, the CC mode stays almost constant up to 80% SoC. After that, the graph shows a significant sharp decrease in the slope of the current and the voltage becomes constant. The current is not exactly constant in CC mode because it has been calculated from the power and voltage profiles. Moreover, the battery voltage of 800 V batteries also exhibits a linear increase, starting from 720 volts at 5% of SoC and reaching a maximum of 820 volts at 80% SoC. The current remains also constant from 10% of SoC, similar to the 400 V battery profile. The CV mode begins after the 80% of

SoC, as shown in Fig. 5c.

The efficiency of charging 400 V and 800 V EVs is shown in Fig. 6a and 6b, respectively, based on modeling semiconductor power losses in PLECS at the switching frequency of 100 kHz with models of SiC MOSFETs employed. The efficiency of a converter is fundamentally determined by its losses, particularly semiconductor losses and transformer losses. In this configuration of 400 V, reconfigurable converter 2 exhibits the highest efficiency, reaching approximately 96%. Following closely behind is reconfigurable converter 1, with an efficiency of around 94%. However, the conventional DAB converter demonstrates comparatively lower efficiency, approximately 86%. Similarly, in the 800 V charging profile, the efficiency versus SoC relation is shown in Fig. 6b. Here, reconfigurable converter 1 emerges as the most efficient, with an efficiency of 99.5%. It is closely followed by the conventional DAB converter, which achieves 99% efficiency. However, in the case of the 800 V charging profile, reconfigurable converter 2 demonstrates lower efficiency due to operating in S mode, leading to additional semiconductor and transformer losses.

V. Conclusion

The efficiency analysis reveals significant differences among the DAB-based converters across 400 V and 800 V charging profiles. Reconfigurable converter 2 demonstrates the highest efficiency of approximately 96% in the 400 V profile, operating in parallel mode to minimize losses. Reconfigurable converter 1 closely follows with an efficiency of around 94%, offering versatility for both 400 V and 800 V profiles. However, the conventional DAB converter exhibits comparatively lower efficiency, averaging around 86% in the 400 V profile. The converter exhibits high efficiency when operated at a 1:1 ratio, which is the turn ratio of its high-frequency transformer, but experiences lower efficiency at a 2:1 ratio.

Acknowledgment

This project has received funding from the European Union's Framework Programme for Research and Innovation, Horizon 2020 (2014-2020), under the Marie Sklodowska-Curie Grant Agreement No. 955614, and from the Helmholtz Association within the Helmholtz Young Investigator Group "Hybrid Networks" (VH-NG-1613).

References

[1] G. Arena, P. Emiliani, A. Chub, D. Vinnikov, and G. De Carne, "Dc fast charging of electric vehicles: a review on architecture and power conversion technology," in *2023 IEEE 17th International Conference on Compatibility, Power Electronics and Power Engineering (CPE-POWERENG)*, pp. 1–6, IEEE, 2023.

[2] I. Aghabali, J. Bauman, P. J. Kollmeyer, Y. Wang, B. Bilgin, and A. Emadi, "800-v electric vehicle powertrains: Review and analysis of benefits, challenges, and future trends," *IEEE Transactions on Transportation Electrification*, vol. 7, no. 3, pp. 927–948, 2020.

[3] C. Jung, "Power up with 800-v systems: The benefits of upgrading voltage power for battery-electric passenger vehicles," *IEEE Electrification Magazine*, vol. 5, no. 1, pp. 53–58, 2017.

[4] G. Rizzoli, M. Mengoni, L. Vancini, G. Sala, A. Tani, and L. Zarri, "Integrated boost-converter for 400 v-800 v fast-charging compatibility," in *2022 Second International Conference on Sustainable Mobility Applications, Renewables and Technology (SMART)*, pp. 1–8, IEEE, 2022.

[5] G. Arena, G. Aiello, G. Scelba, M. Cacciato, and F. Gennaro, "A cost-effective hardware in the loop implementation of dual active bridge for fast prototyping of electric vehicles charging controls," in *2021 23rd European Conference on Power Electronics and Applications (EPE'21 ECCE Europe)*, pp. P–1, IEEE, 2021.

[6] G. Arena, D. Vinnikov, A. Chub, and G. De Carne, "Accuracy analysis of dual active bridge simulations under different integration methods," in *2022 AEIT International Annual Conference (AEIT)*, pp. 1–6, IEEE, 2022.

[7] G. Arena, A. Chub, M. Lukianov, R. Strzelecki, D. Vinnikov, and G. De Carne, "A comprehensive review on dc fast charging stations for electric vehicles: Standards, power conversion technologies, architectures, energy management, and cybersecurity," *IEEE Open Journal of Power Electronics*, 2024.

[8] Z. Qin, Y. Shen, P. C. Loh, H. Wang, and F. Blaabjerg, "A dual active bridge converter with an extended high-efficiency range by dc blocking capacitor voltage control," *IEEE Transactions on Power Electronics*, vol. 33, no. 7, pp. 5949–5966, 2017.

[9] O. Zayed, A. Elezab, A. Abuelnaga, and M. Narimani, "A dual-active bridge converter with a wide output voltage range (200-1000 v) for ultra-fast dc-connected ev charging stations," *IEEE Transactions on Transportation Electrification*, 2022.

[10] Ö. Ekin, G. Arena, S. Waczowicz, V. Hagenmeyer, and G. De Carne, "Comparison of four-switch buck-boost and dual active bridge converter for dc microgrid applications," in *2022 IEEE 13th International Symposium on Power Electronics for Distributed Generation Systems (PEDG)*, pp. 1–6, IEEE, 2022.

[11] A. Kadavelugu, S. Baek, S. Dutta, S. Bhattacharya, M. Das, A. Agarwal, and J. Scofield, "High-frequency design considerations of dual active bridge 1200 v sic mosfet dc-dc converter," in *2011 Twenty-Sixth Annual IEEE Applied Power Electronics Conference and Exposition (APEC)*, pp. 314–320, 2011.

[12] S. Ji, S. Zheng, Z. Zhang, F. Wang, and L. M. Tolbert, "Protection and temperature-dependent switching characterization of latest generation 10 kv sic mosfets," in *2017 IEEE Applied Power Electronics Conference and Exposition (APEC)*, pp. 783–788, IEEE, 2017.

[13] K. Venkatachalam, C. R. Sullivan, T. Abdallah, and H. Tacca, "Accurate prediction of ferrite core loss with nonsinusoidal waveforms using only steinmetz parameters," in *2002 IEEE Workshop on Computers in Power Electronics, 2002. Proceedings.*, pp. 36–41, IEEE, 2002.

[14] M. K. Kazimierczuk, *High-frequency magnetic components*. John Wiley & Sons, 2009.

[15] K. Liu, K. Li, Q. Peng, and C. Zhang, "A brief review on key technologies in the battery management system of electric vehicles," *Frontiers of mechanical engineering*, vol. 14, pp. 47–64, 2019.